

# The Stability Diagram of a Few Electron Artificial Triatom

Louis Gaudreau<sup>1,2</sup>, Sergei Studenikin<sup>1</sup>, Andy Sachrajda<sup>1</sup>, Piotr Zawadzki<sup>1</sup>, Alicia Kam<sup>1</sup>,  
Jean Lapointe<sup>1</sup>, Marek Korkusinski<sup>1</sup> and Pawel Hawrylak<sup>1</sup>

<sup>1</sup>Institute For Microstructural Sciences, NRC, Ottawa, Canada K1A 0R6

<sup>2</sup>Réseau Québecois sur les Matériaux de Pointe,  
Université de Sherbrooke, Quebec, Canada J1K 2R1

**Quantum dots are considered building blocks for future quantum information circuits. We present here experimental results on a quantum dot circuit consisting of three quantum dots with controlled electron numbers down to one per dot and tunable coupling. We experimentally map out for the first time the stability diagram of the triatomic system and reveal the existence of quadruple points, a signature of the three dots being in resonance. In their vicinity we observe a surprising effect, a ‘cloning’ of charge transfer transitions related to charge and spin reconfigurations. The experimental results are reproduced by equivalent circuit analysis and Hubbard models.**

In recent years, a comparison between single quantum dots and real atoms (1) has confirmed both similar and significantly different properties. Atomic-like shell structure has been observed (2,3). On the other hand, the very different energy scales of the artificial atom manifests itself in novel interaction phenomena which have no analogue in real atoms, such as singlet triplet transitions and spin texture arrangements of electrons (4,5). Recently, with the realization of electrostatic few-electron quantum dots (6) and their combination with non-invasive charge detection technology (7), tunable coupled few electron quantum dots (i.e. artificial diatomic molecules) have been studied. In addition to fundamental studies of quantum molecular effects, the tunability of these devices makes them promising candidates for future quantum information applications (8-10,11-13) and studying novel nanospintronic functionalities (14). If techniques can be developed to further exploit the complexity of these systems by coupling larger numbers of dots with a controlled number of electrons together, new regimes of ‘artificial quantum matter’ with resulting new phenomena, should become accessible. There has, indeed, been growing theoretical interest in the next level of complexity, the few-electron triple dot or triatom. Rectification and ratchet functionalities have been predicted (15,16) for this system as well as applications in the field of quantum information as entanglers (11) or coded qubits (10,12,13). We present here the first experimental results from an artificial triatom.

The starting point for any experimental investigation of such a complex system is the stability diagram, i.e. the map of the electron configurations. In this paper we reveal the properties of the stability diagram of an artificial triatom. We find that it is characterised both by quadruple points and a new element resulting from internal charge and spin rearrangements. A dramatic manifestation of this effect within the stability

diagram is the *cloning* of charge transfer boundaries. Charge transfer boundaries are observed when electron configurations change at a fixed total electron number. We concentrate on the most fundamental quadruple points of the system, in which one, two, or three electrons are shared between the dots. While these results will need to be taken into account when designing either charge or spin qubit implementation schemes, they also provide novel functionalities and new opportunities for processing and moving quantum information around a circuit. Additionally, this phenomenon may be considered a basic demonstration of a QCA effect in a few electron regime and may form the basis of future QCA architectures (17,18).

Achieving an artificial triatom is extremely challenging. Ciorga et al.(6) first demonstrated that a single electron could be isolated from a two dimensional electron gas in an AlGaAs/GaAs heterostructure with a suitable lateral electrostatic gate layout. Soon after this, two coupled few electron quantum dots were realized by several groups (14,19-25). Further developing this layout for more than two artificial atoms is topologically not trivial. An alternative approach is to take advantage of the tunability of the incidental potential profile or of the metallic gate structure in dividing a single electrostatically defined dot into two. This has been already demonstrated by Ciorga et al.(26) who showed that the charge in a single dot can be separated into two spatial regions at high magnetic fields, and by Huttel et al. (27) who demonstrated that a single dot could be purposely split into two tunable confining potentials using appropriate gate operations. In this work we achieve our triatom by a combination of these capabilities, i.e. we use the coupled quantum dot potential design but with voltages applied so that one of the two confinement regions is divided into a potential profile with two minima forming two smaller quantum dots. Modeling of the confining potential of our device confirmed the possibility of dividing the potential into a 3-dot arrangement by using suitable gate voltages. However, on three separate cooldowns the few electron triatom required different voltages to be applied to the gates thereby confirming an influence of intrinsic potential fluctuations. Experimentally, this emphasizes the importance of charge detection technology in calibrating these complex devices after a cooldown. A schematic of the resultant triatom is shown in the inset of figure 1. All three dots A, B and C are coupled to each other. Figure 1 also shows a quantum point contact (QPC) charge detector used to probe the triatom. We employ charge detection, since the experimental condition to observe transport through three quantum dots is very restrictive. The current through the QPC (I<sub>QPC</sub>) is sensitive to any change in the triatom charge configuration. The derivative  $\partial I_{QPC} / \partial V_{4B}$  is measured using standard low frequency AC techniques.

In general, the stability diagram for an arrangement of N coupled dots is an N-dimensional entity. This provides experimental difficulties for N>2. However, we can take advantage of the property that all controlling gates are to some degree capacitively coupled to all dots. The consequence of this cross capacitance is that any 2D slice through the stability diagram should reveal N sets of parallel Coulomb blockade lines (ignoring for the moment behaviour at crossing points). Each set reflects the occurrences when the electrochemical potential of the leads and a particular dot are matched. For the triatom this predicts three sets of negatively sloped parallel lines. In a random slice the crossing points would in all probability involve only two of the sets of lines, i.e. the triple

points studied in experiments on coupled quantum dots(14,19-25). To observe triatomic features, it is necessary to achieve very particular slices in which lines from all three sets cross each other at a single location, called the quadruple point.

Figure 1 shows an experimental 2D stability diagram of the triatom plotted as a colour scale graph. The behaviour predicted above is confirmed. The three sets of parallel lines with negative slopes marked by red, blue and green circles refer to changing the number of electrons in A, B and C respectively. The spacing between parallel lines, related to charging energy, is smallest for dot C due to the respective dot sizes. Gate 5B primarily affects C while Gate 1B mainly affects A and B. The three ovals are drawn to indicate triple points associated with the three possible combinations of two dots. The spacing and curvature of the lines confirms that for this random slice A and B are coupled more strongly than A and C, and B and C. We note the successful realization of the fundamental configurations (0,0,0) and (1,1,1) where  $(N_A, N_B, N_C)$  refer to the occupation number of the A,B,C dots.

To realize the quadruple points experimentally, the gate voltages need to be adjusted to merge two triple points. This has been achieved experimentally by tuning voltages  $V_{3T}$  and  $V_{3B}$  and is shown in detail in figures 2(a) to 2(e). Crossing certain lines involves a change in the total number of electrons, the slope and the amplitude can be used to identify the dot into which the electron is being added. A second category of line indicates a charge reconfiguration at a fixed total electron number, for example from (0,1,0) to (0,0,1). The charge reconfiguration occurs when the electrochemical potential of two dots are matched. For features related to two coupled dots the charge transfer lines span two triple points. The blue circle in Fig.2 marks a triple point between A and B in which both configurations (0,1,0) and (0,0,0) are degenerate with (1,0,0). The pink circle is a triple point between B and C for which (0,1,0), and (0,0,0) are also degenerate but with (0,0,1). To observe a quadruple point, the blue and pink points must be made to coincide. In figure 2(a) these points are still far apart. A charge transfer line is marked by a dotted line for clarity ((1,0,0) to (0,1,0)). In figure 2(b) the two triple points are moved closer together. On close inspection of figure 2(b) a new feature is emerging close to the C=1 line (the line corresponding to the addition of the first electron into C) at the division between (0,1,0) to (0,1,1) states. In figure 2(c) it is seen that this extra feature has evolved into a new additional charge transfer line which is parallel to the one between (1,0,0) and (0,1,0). We, therefore, refer to it as a clone of the original line. Based on the models presented below the configurations on either side of the clone line are identified as (1,0,1) and (0,1,1). In figure 2(d) we observe that the original charge transfer line between (1,0,0) and (0,1,0) has disappeared but the clone still exists. Finally, in figure 2(e) the cloning sequence repeats itself as the charge transfer line crosses the C=2 line, at which a second electron is injected into dot C.

Figure 3 shows the results of an equivalent circuit model (28), in which the electrostatic energy of the triatom is given by

$$E_{triatom} = \sum_{i=1}^3 \left( \frac{1}{2} U_i N_i^2 \right) + \sum_{i < j, j=2}^3 N_i N_j U_{i,j} + f(V_{1B}, V_{5B}), \text{ where } N_i \text{ is the number of electrons in dot } i, U_i \text{ is its charging energy, } U_{i,j} \text{ is the capacitive coupling energy between dots } i \text{ and } j.$$

$j$ , and  $f$  is the electrostatic energy due to the gate voltage induced charge. The ratios of charging and capacitive coupling energies were extracted directly from the data in Fig.2 and fed into the model. Specifically,  $U_1 = 3.1$  meV,  $U_2 = 2.8$  meV,  $U_3 = 2.28$  meV,  $U_{12} = 0.86$  meV,  $U_{13} = 0.28$  meV,  $U_{23} = 0.57$  meV. This leaves only the ground state energies of each dot as fitting parameters for the model. To include quantum effects we also describe the triatom by an effective Hubbard model. This model also includes tunnelling and the Pauli exclusion principle. With  $c_{i\sigma}^+$  ( $c_{j\sigma}$ ) operators describing creation (annihilation) of electron on the lowest energy level  $E_i$  of the  $i^{\text{th}}$  dot ( $i = 1, 2, 3$ ), the Hubbard Hamiltonian can be written as  $H = \sum_{ij\sigma} (E_i \delta_{ij} + t_{ij}) c_{i\sigma}^+ c_{j\sigma} + \sum_i U_i n_{\uparrow i} n_{\downarrow i} + \sum_{i < j} V_{ij} n_i n_j$ , where

$n_{\uparrow i} = c_{i\uparrow}^+ c_{i\uparrow}$  and  $n_i = n_{\uparrow i} + n_{\downarrow i}$  is spin and charge density in dot “ $i$ ”. The first term

describes the energy of each dot and the interdot tunneling  $t_{ij}$ , which were obtained from the experimental data,  $t_{13} = t_{23} = 9.7$   $\mu$ eV,  $t_{12} = 67.8$   $\mu$ eV, and used in the model. The second term describes the charging energy  $U_i$ . The last term describes the interaction energy between electrons occupying different dots. To make contact with experiment, we assume that the energies  $E_i$  are linear functions of gate voltages; other Hubbard parameters are extracted from experiment. The ground-state energy  $E_0$  is obtained by diagonalizing the Hubbard Hamiltonian. We use these energies to calculate the chemical potential of the triatom  $\mu(N) = E_0(N+1) - E_0(N)$ . When  $\mu(N)$  equals the chemical potential of the leads, the  $N+1^{\text{st}}$  electron is added. This establishes the triatom stability diagram as a function of applied voltages. From the corresponding ground-state wave function we establish the occupation  $n_A, n_B, n_C$  of each dot and compute the QPC voltage  $V_{QPC} \sim n_A/R_A + n_B/R_B + n_C/R_C$ , with  $R_A, R_B, R_C$  being respectively the distances of the A, B, and C dots from the QPC. Addition of an extra electron or rearrangement of the electronic charges results in a change of  $V_{QPC}$ , or a peak in its derivative. Figures 3(b) and 3(c), which should be compared with figure 2(c), show the results from the two models with quantum effects leading to smearing and curvature of the charge addition and transfer lines. The cloning of the charge transfer line is indeed predicted by both models. The resulting configurations are indicated in the figures.

The origin of the clone line is revealed as a charge re-arrangement effect, reminiscent of QCA. This is shown in more detail in figure 4(a). Starting from the left the following sequence of events occurs. Initially a single electron resides in A. As gate 5B is made less negative it becomes energetically favorable for the electron to transfer to B. As the gate sweep continues, the triatom enters the two-electron regime. This transition involves a more complex, two-step process (reminiscent of a quantum cellular automata effect). When the second electron enters C, the electron in B immediately reverts back to A. This is a consequence of the difference in interdot coupling between A and C, and B and C due to their spatial locations. It is important to note that the effect is in fact quite universal, e.g. inverting the interdot couplings would involve making geometrical changes that would simply switch the roles of A and B. Finally, as the gate is swept further, the electron in A is once again transferred into B. This latter event is the origin of the clone line. It is parallel to the first charge transfer line since they both involve the transfer of an electron from A to B, the only difference being the presence of an electron in C. The disappearance of the original charge transfer line at the C=1 line is now also

clear. The configuration on crossing the  $C=1$  line is uniquely the  $(1,0,1)$  state for both the initial  $(1,0,0)$  and  $(0,1,0)$  configurations. We also note that in both the experiment and the models, the slope of the  $C=1$  line is different between the two quadruple points marked  $\alpha$  and  $\beta$  in fig.4(a). The model also explains the behaviour of the slopes of two neighbouring charge transfer lines marked by  $\gamma$  and  $\delta$  in figure 2(a). These are the lines obtained when transferring an electron into an empty dot C from A or B. Comparing figure 2(a) and 2(d) the  $\gamma$  and  $\delta$  slopes are reversed. But in 2(c) they have exactly the same slope. This behaviour is consistent with the configurations. In 2(a),  $\gamma$  ( $\delta$ ) refer to a transfer of an electron from A (B) to C. But in 2(c), as a result of the charge reconfiguration effect, both lines involve a transfer of an electron from B into C resulting in similar slopes. We have noticed that the clone line has a slightly different slope when it starts to appear (figs. 2(b) and 2(e)), and evolves into a perfect clone of the original charge transfer line; this feature remains unexplained by both models.

The two quadruple points, marked  $\alpha$  and  $\beta$ , in figure 4(a) are observed simultaneously. The nature of this coincidence remains unclear. At the quadruple point  $\alpha$  the ‘vacuum’ state  $(0,0,0)$  is resonant with the three single electron configurations  $(1,0,0)$ ,  $(0,1,0)$  and  $(0,0,1)$ . At quadruple point  $\beta$  the  $(1,1,1)$  configuration is resonant with the three double occupied states  $(1,1,0)$ ,  $(0,1,1)$  and  $(1,0,1)$ . In fact we are able to realize many other quadruple points experimentally by gate adjustments, opening up a new playground for fundamental studies of complex entangled quantum states. The  $(1,1,1)$  region, for example, is a necessary condition to create the Greenberger-Horne-Zeilinger maximally entangled states which will enable quantum algorithms, such as quantum teleportation implemented (29). The cloning of charge transfer lines occurs at other crossing points of the triatom stability diagram. Some of these are expected to involve simultaneous charge and spin rearrangements. Figure 4(b), for example, plots the equivalent behaviour at such a location. The charge rearrangement in this case involves the transition from  $(0,2,0)$  to  $(1,1,1)$  which, at low magnetic fields, one would expect to be accompanied by a spin flip event (4,25). While at higher fields (above the singlet-triplet transition for two electrons in dot B) this should not be the case. The schematics indicate the distribution of electrons amongst the dots. We note that the observation of quadruple points and cloned lines are closely linked. The latter requires the energy mismatch of two dots to be small relative to the difference in their Coulomb coupling to the third dot which itself needs to be close to resonance with the electron leads. This condition can only occur around quadruple points.

In conclusion, the stability diagram of a few-electron artificial triatom has been measured for the first time. The most fundamental quadruple degeneracies were realized. The results reveal a new playground for fundamental physics and quantum applications. The stability diagram of a triatom is found to be a complex object containing charge and spin rearrangements in the vicinity of quadruple points. These rearrangements may lead to applications in QCA circuits as well as in quantum information implementation schemes.

## References and notes

1. R. C. Ashoori, *Nature* **379**, 413 (1996).
2. S. Tarucha, *et al.*, *Phys. Rev. Lett.* **77**, 3613 (1996).
3. S. Raymond, *et al.*, *Phys. Rev. Lett.* **92**, 187402 (2004).
4. L. P. Kouwenhoven, *et al.*, *Science* **278** (1997)
5. M. Korkusinski, *et al.*, *Phys. Rev. Lett.* **93**, 206806 (2004).
6. M. Ciorga *et al.*, *Phys. Rev. B* **61**, R16315 (2000).
7. M. Field *et al.*, *Phys. Rev. Lett.* **70**, 1311 (1993).
8. D. Loss, D. P. DiVincenzo, *Phys. Rev. A* **57**, 120 (1998).
9. D. P. DiVincenzo *et al.*, *Nature* **408**, 339 (2000).
10. T. Tanamoto, *Phys. Rev. A* **61**, 022305 (2000).
11. D. S. Saraga, D. Loss, *Phys. Rev. Lett.* **90**, 166803 (2003).
12. A. Mizel, D. A. Lidar, *Phys. Rev. Lett.* **92**, 077903 (2004).
13. P. Hawrylak, M. Korkusinski, *Sol. St. Comm.* **136**, 508 (2005).
14. M. Pioro-Ladrière *et al.*, *Phys. Rev. Lett.* **91**, 026803 (2003).
15. M. Stopa, *Phys. Rev. Lett.* **88**, 146802 (2002).
16. A. Vidan *et al.*, *Appl. Phys. Lett.* **85**, 3602 (2004).
17. G. Toth, C. S. Lent, *Phys. Rev. A* **63**, 052315 (2001).
18. I. Amlani *et al.*, *Science* **284** 289 (1999)
19. C. Livermore *et al.*, *Science* **274**, 1332 (1996).
20. T. H. Oosterkamp *et al.*, *Nature* **395**, 873 (1998).
21. A. W. Holleitner *et al.*, *Science* **297**, 70 (2001).
22. J. M. Elzerman *et al.*, *Phys. Rev. B* **67**, 161308 (2003)
23. J. R. Petta *et al.*, *Phys. Rev. Lett.* **93**, 186802 (2004)
24. M. Pioro-Ladrière *et al.*, *Phys. Rev. B* **72**, 125307 (2005)
25. J. R. Petta *et al.*, *Science* **30**, 2180 (2005).
26. M. Ciorga, *et al.*, *Proceedings of ICPS-26*, St. Andrews (2002)
27. A. K. Hüttel *et al.*, *Phys. Rev. B* **72**, 081310 (2005).
28. A. Vidan *et al.*, *Journal of Superconductivity : Incorporating Novel Magnetism* **18** 223 (2005)
29. M. A. Nielsen, E. Knill, R. Laflamme, *Nature* **396**, 52 (1998).
30. A.S. acknowledges financial support from the Natural Sciences and Engineering Research Council of Canada and A.S., P.H. and A. Kam acknowledge support from the Canadian Institute for Advanced Research. The authors thank K. Le Hur and M. Pioro-Ladrière for discussions.

## Figure legends

**Fig. 1** Stability diagram of the triatom, mapping electron configurations as a function of applied gate voltages. Three different sets of parallel lines are observed, each one corresponding to the addition spectrum of a dot: A (red), B (blue) and C (green). Dashed ovals correspond to three different triple points, where the chemical potentials of two dots

and the leads coincide. **Inset** Scanning electron micrograph of a device, schematically indicating the position of the three dots. The dots are created by electrostatic confinement using metallic gates (1B, 2B, 3B, 4B, 5B, 3T) placed 90 nm above a GaAs/AlGaAs heterostructure containing a two-dimensional electron gas. Gate S is used as a QPC charge detector, with which we monitor the electronic configurations and rearrangements in the triatom by measuring its transconductance  $dI_{QPC}/dV_{4B}$ .

**Fig. 2** Evolution of the triatom in the (0,0,0) to (1,1,1) region as two triple points are gradually merged. Dashed lines have been drawn over inter-dot charge transfer lines for clarity. **a** Triple points where dots A and B are in resonance (light blue circle) and dots B and C are in resonance (pink circle), relatively far from one another. **b** The two triple points are closer together and a new structure starts to appear on the right side of the C=1 line. **c** The two triple points coincide, creating a quadruple point where the three dots are in resonance. We observe the appearance of a new line on the right side of the C=1 line. **d** The triple points move apart again, the original charge transfer line has disappeared, while the new one remains. **e** The charge transfer line duplicates again as the C=2 line is crossed.

**Fig. 3** Theoretical models for the triatom. **a** Schematics of the triatom's circuit model where all dots are capacitively coupled. **b** Theoretical stability diagram using the equivalent circuit model where all parameters are extracted from experimental data. The cloning of the charge transfer line is predicted by the model, indicating charge reconfiguration within the triatom as an extra electron is added to dot C. **c** Theoretical

stability diagram using a Hubbard model, including tunneling energies between dots, which were also extracted from experimental data. Again, the cloning of the charge transfer line is predicted by this model.

**Fig. 4** Schematic evolution of the triatom configuration in the vicinity of two different quadruple points as gate 5B is made less negative. **a** Starting with one electron in A (far left) (1,0,0), the electron is transferred to B (0,1,0), the addition of an extra electron to C triggers an electronic rearrangement in the other dots and the first electron is transferred from B to A (1,0,1), finally the electron is retransferred from A to B (0,1,1) . **b** Starting with one electron in A and 1 electron in B (1,1,0), the electron from A is transferred to B (0,2,0), the addition of an extra electron in C creates again a charge rearrangement (1,1,1), but this time involving a spin rearrangement at low magnetic fields. Finally an electron is transferred from A to B again (0,2,1).

Fig. 1

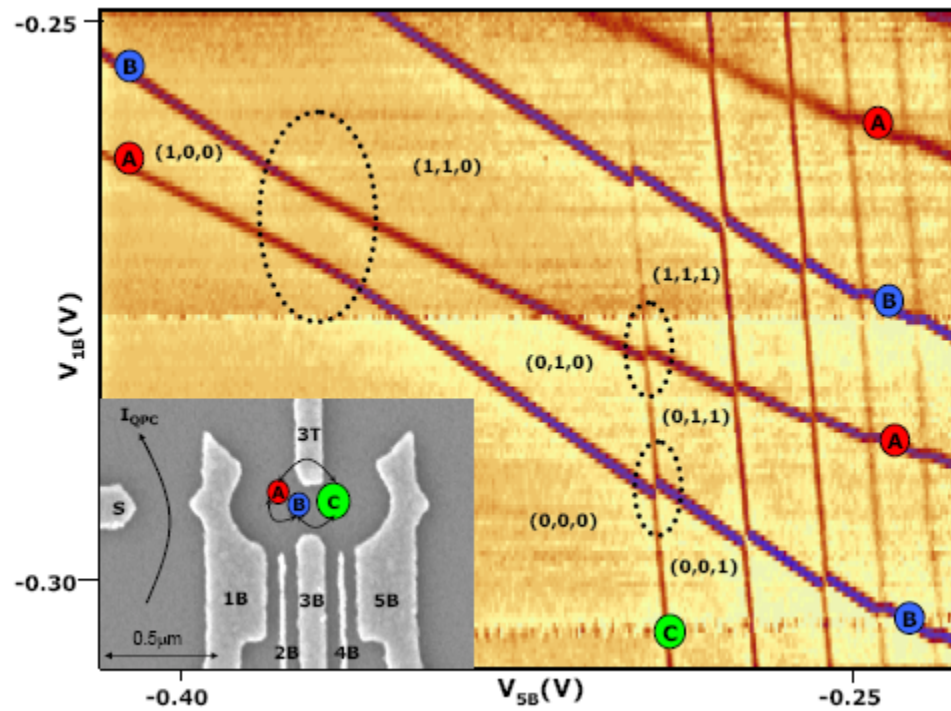


Fig.2

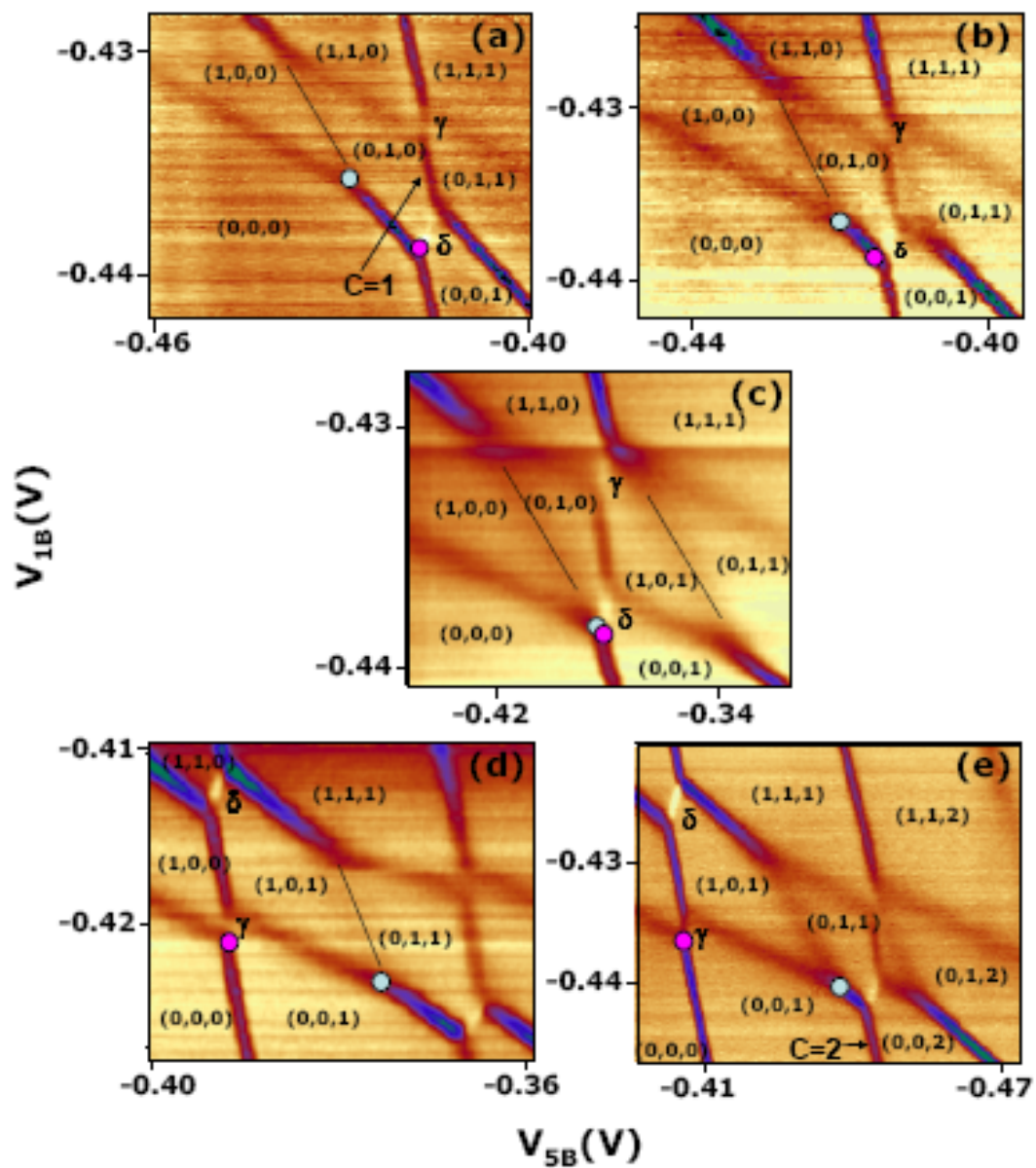


Fig. 3

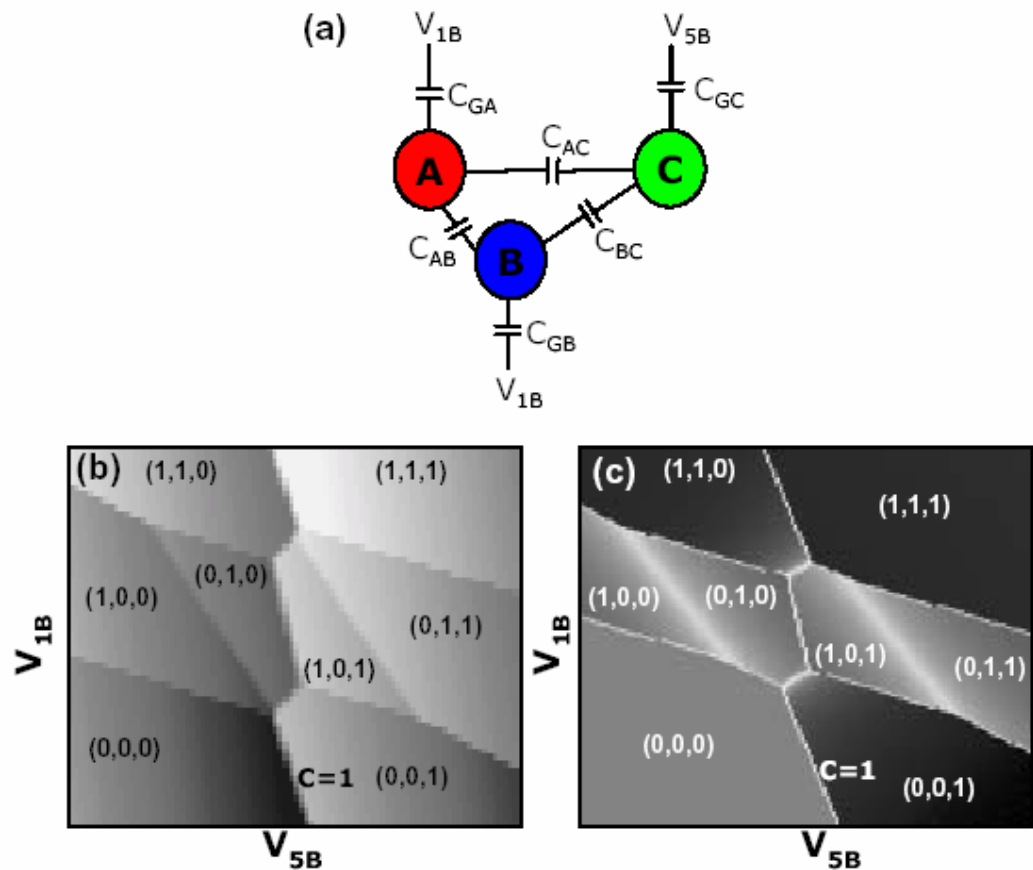


Fig. 4

